Available online at www.sciencedirect.com
ScienceDirect
Journal of the European Ceramic Society 27 (2007) 951–958
www.elsevier.com/locate/jeurceramsoc

$CoAl_2O_4$–mullite composites prepared by sol–gel processes

Stanislav Kurajica [a], Emilija Tkalcec [a,*], Joerg Schmauch [b]

[a] *Faculty of Chemical Engineering and Technology, University of Zagreb, Marulicev trg 20, HR-10000 Zagreb, Croatia*
[b] *University of Saarland, FR 7 3, D-66041 Saarbruecken, Germany*

Available online 9 June 2006

Abstract

The formation of $CoAl_2O_4$–mullite composites from diphasic sol–gel precursors with 3:2 mullite composition doped with 1, 2 and 3 at.% Co^{2+} was studied by differential scanning calorimetry (DSC), X-ray diffraction and Rietveld structure refinement. The course of thermal reactions is dominated by the intermediate formation of two faint crystallized phases having different composition and activation energies. The former phase with smaller activation energy (822 kJ mol^{-1}) is attributed to cobalt-containing spinel structure and the latter with larger activation energy (about 1200 kJ mol^{-1}) to Al–Si spinel. With temperature increase Co-containing spinel transforms progressively in $CoAl_2O_4$, while Al–Si spinel forms mullite above 1100 °C. Mullite lattice parameters, Rietveld refinement data and the $CoAl_2O_4$/Co^{2+} ratio in annealed samples points out that the majority of cobalt is incorporated in $CoAl_2O_4$ and only about 0.6 at.% enters mullite structure or the glassy phase, or both.

Keywords: Sol–gel processes; Nanocomposites; X-ray methods; Mullite; Spinels

1. Introduction

The high strength at high temperature, low thermal expansion and outstanding chemical stability make mullite, $3Al_2O_3{\cdot}2SiO_2$, an attractive ceramic material for advanced applications.[1] Recently, variety of mullite matrix composites have been intensively studied, some of them yielding improved mechanical properties. Chemical routes for the synthesis of mullite-composites are proving to be highly efficient and versatile in tailoring the elemental combination and intrinsic properties of the composites. Depending on the starting materials and methods applied, the synthesized precursors have different properties, which in turn affect the resulting properties of the ceramics. A wide variety of transition metals enter the mullite structure. Schneider et al.[2] have performed a systematic study in order to determine the solubility limit of various transition metal ions, as well as, the location of corresponding cations in the structure. The solubility limit depends on radii and oxidation states of the transition metal ions. Trivalent cations with ionic radii close to that of Al^{3+} can readily be incorporated in mullite structure. As shown recently[3–5] divalent cations (Me) with larger ionic radii rather react with alumina forming $MeAl_2O_4$ than enter to mullite structure. Spinels containing transition metal ions can act as efficient catalysts in various heterogeneous chemical processes, or selective oxidation and reduction agents of several organic molecules. Most transition metal oxides form the same type of spinel phase with alumina. Cobalt aluminate, $CoAl_2O_4$, with the normal spinel structure has been known since ancient times as ceramic pigment and has often attracted the attention of researchers.[6] Recently nanosized $CoAl_2O_4$ and Al_2O_3–$CoAl_2O_4$ s.s. spinels by sol–gel method were prepared.[7] So, it appeared interesting to see the influence of Co^{2+} on the crystallization scheme of mullite in diphasic gels where Al–Si spinel is forming as an intermediate phase.

The aim of the work was to study the thermal evolution and kinetics of in situ formed $CoAl_2O_4$–mullite composites by sol–gel synthesis. Diphasic gels in which 1, 2 and 3 at.% of aluminum is substituted by Co^{2+} cation were prepared by mixing nitrate solutions with tetraetoxysilane (TEOS). The structural evolution with temperature has been studied by differential scanning calorimetry (DSC) and X-ray diffraction (XRD) analysis and Rietveld structure refinement. The microstructure and morphology of formed $CoAl_2O_4$–mullite composites were investigated by scanning electron microscopy (SEM) and energy dispersive X-ray spectrometry (EDXS).

* Corresponding author. Tel.: +385 1 4597 219; fax: +385 1 4597 250.
E-mail address: etkalcec@fkit.hr (E. Tkalcec).

0955-2219/$ – see front matter © 2006 Elsevier Ltd. All rights reserved.
doi:10.1016/j.jeurceramsoc.2006.04.127

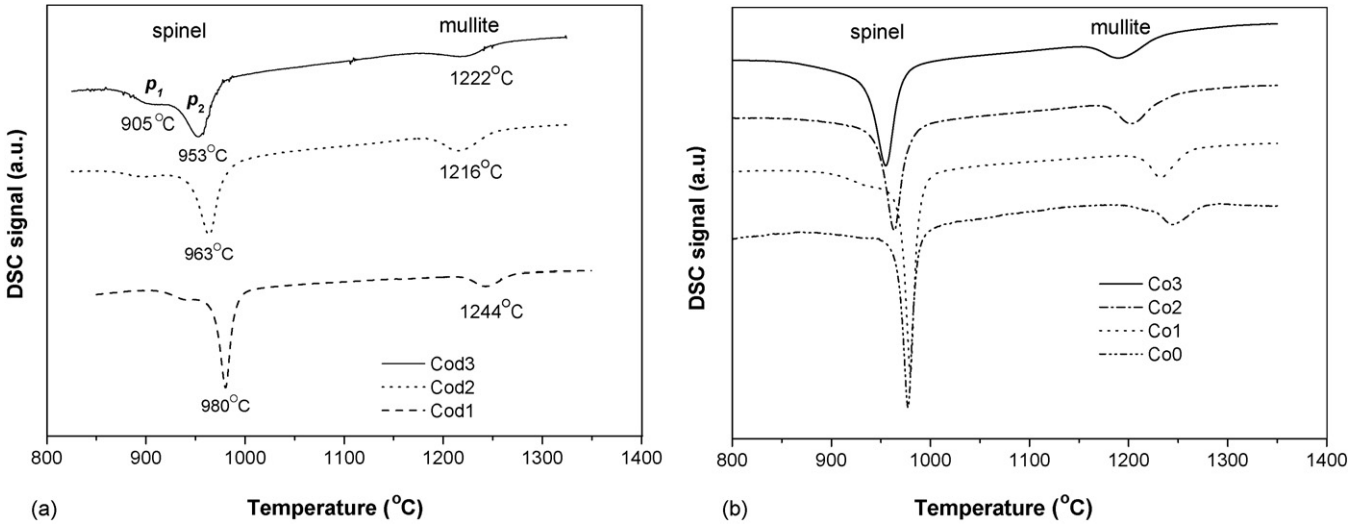

Fig. 1. DSC scans of (a) dried gels (120 °C for 72 h) and (b) calcined gels (700 °C for 2 h).

2. Experimental procedure

2.1. Gel preparations

Non-doped diphasic gel with $3Al_2O_3{\cdot}SiO_2$ (nominal) composition and gels doped with 1, 2 and 3 at.% Co^{2+} (introduced on account of Al^{3+}) were prepared by dissolving nitrates, $Al(NO_3)_3{\cdot}9H_2O$ and $Co(NO_3)_2{\cdot}6H_2O$ in water, and by mixing nitrate solutions with tetraetoxysilane (TEOS) dissolved in ethanol. TEOS solution was added dropwise under vigorous stirring. The mixture was stirred under reflux conditions at 60 °C for 8 days. The gels were dried at 120 °C for 72 h, ground and sieved. For further analyses powders with particle size <63 μm were used. Two sets of gels were prepared: dried and calcined. Dried gels were denoted as Cod1, Cod2 and Cod3, whereas gels calcined at 700 °C for 2 h as Co1, Co2 and Co3 samples.

2.2. Methods

Differential scanning calorimetry (DSC) was performed on a Netzsch STA 404 Simultaneous Thermal Analyzer used in DSC mode. Pt pans and corundum as a standard were used. In order to assign the exothermic peaks on DSC scan to each individual crystalline phase, DSC analysis was performed at the rate of 10 K min^{-1}. The analysis was stopped successively at higher temperature, the sample was quenched and analyzed by X-ray diffraction analysis (XRD). For the purpose of evaluation the crystallization kinetic parameters, DSC analysis was performed at five different heating rates (5, 7 10, 15 and 20 K min^{-1}). The activation energy of crystallization is calculated using Kissinger equation[8]:

$$\ln\left(\frac{\beta}{T_p^2}\right) = -\frac{E_a}{RT_p} + C \quad (1)$$

where β is the heating rate (K min^{-1}), E_a the activation energy of crystallization (kJ mol^{-1}), R the gas constant, T_p the exothermic peak temperature K and C is a constant.

Computer controlled diffractometer Siemens D 500/PSC with Cu Kα radiation, with quartz single crystal monochromator and a curved position sensitive detector was used for XRD analysis. Data were collected between 5° and 70° 2θ in a step scan mode with steps of 0.02° and counting time of 3 s. For the purpose of the Rietveld structure refinement,[9] the XRD data were collected on diffractometer (Philips PW1710) in the range from 10° to 100° 2θ (Cu Kα) in steps of 0.02° and fixed counting time of 10 s per step. Rietveld structure refinement was carried out on XRD patterns of samples heat treated at 1600 °C for 2 h using Topas 2.1 program.[10] The structural models for mullite, $CoAl_2O_4$ and corundum were based on the data reported in references.[11–13] The refinement started in the space group *Pbam* with mullite structure without cobalt incorporation.[11] For the case of Co^{2+} incorporated into mullite, cobalt atoms replaced a fraction of Al atoms at 2a octahedral site. The morphology of sintered samples were examined using scanning electron microscopy (SEM) and energy dispersive X-ray spectroscopy (EDX) (JEOL, JSM 6400F).

3. Results

3.1. Differential scanning calorimetry and activation energy determination

DSC scans of dried and calcined gels are given in Fig. 1. Dry gels exhibited two exothermic peaks, p1 and p2, in temperature range of spinel crystallization (900–1000 °C) and one peak in temperature range of mullite crystallization (1200–1300 °C). In calcined samples, however, two peaks corresponding to spinel crystallization are overlapped, as shown in Fig. 1b. The temperatures of spinel and mullite crystallization for both sets of samples are given in Table 1. As the peak p1 increases with the increase of cobalt doping level, it is obvious that the first peak is related to a cobalt containing phase. On the other hand, calcined gels (Fig. 1b) exhibited only overlapping peaks in the temperature range of spinel crystallization and the peak attributed to mullite crystallization was enlarged in comparison to dried sam-

Table 1
Effect of Co^{2+} on temperature of spinel and mullite crystallization (T_p) determined by DSC analysis (heating rate 10 K m^{-1})

Sample notation	Thermal treatment	Co^{2+} doped level (at.%)	T_p (°C)	
			Spinel	Mullite
Co0	Calcined	0	977	1247
Cod1	Dried		939; 980	1244
Co1	Calcined	1	980	1228
Cod2	Dried		901; 963	1216
Co2	Calcined	2	963	1203
Cod3	Dried		905; 953	1222
Co3	Calcined	3	955	1189

Gels marked as Cod1, Cod2 and Cod3 are dried at 120 °C for 72 h, and gels marked as Co1, Co2, Co3 were subsequently annealed at 700 °C for 2 h.

ple's scans. Therefore, for the evaluation of the activation energy for spinel crystallization, the DSC scans of dried gels were used. For the evaluation of the activation energy of mullite crystallization, DSC scans of calcined samples were used, as in those scans mullite peaks are better defined. The Kissinger plots[8] [$\ln(\beta/T_p^2)$ versus $1/T_p$] for spinel peaks p1 and p2 are shown in Fig. 2a and those for mullite in calcined samples in Fig. 2b. The activation energies were calculated from the slopes of the linear fits to the experimental data using Eq. (1) and are presented in Table 2. As the spinel peaks p1 on DSC scans of Cod1 and Cod2 samples and mullite peaks on DSC scans of all three dried gels are weak and broad, allowing only approximate determination of T_p, they were not used for the kinetics evaluation. The overlapped spinel peaks on DSC scans of calcined samples were also not suitable for the determination of kinetics parameters, as seen in Fig. 2c.

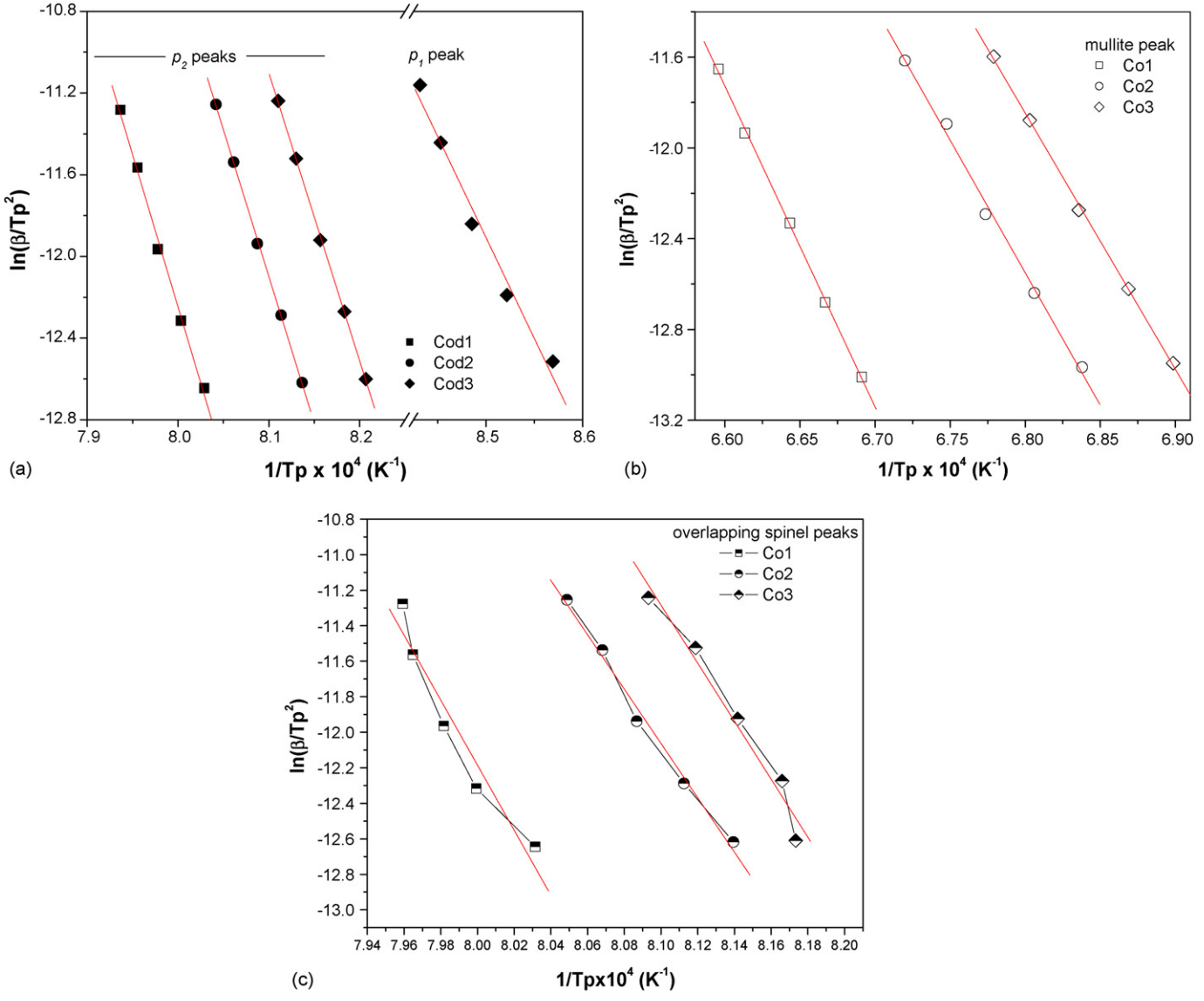

Fig. 2. (a) Kissinger plots for spinel peak p2 for samples Cod1, Cod2 and Cod3 and for spinel peak p1 for Cod3. (b) Kissinger plots for mullite peak; samples Co1, Co2 and Co3. (c) Kissinger plots for overlapped spinel peak; samples Co1, Co2 and Co3.

Table 2
Activation energies of spinel and mullite crystallization

Sample	E_a (kJ mol^{-1})		
	Spinel		Mullite
	Peak p1	Peak p2	
Cod1	Broad[a]	1232 ± 45	Broad[a]
Cod2	Broad[a]	1192 ± 15	Broad[a]
Cod3	822 ± 64	1173 ± 15	Broad[a]
Co1	Overlapped[b]		1175 ± 17
Co2	Overlapped[b]		971 ± 39
Co3	Overlapped[b]		939 ± 15

[a] Due to broad and weak peaks T_p could not be accurately determined.
[b] Due to overlapping of peaks the plot $\ln(\beta/T_p^2)$ vs. $1/T_p$ is not linear (see Fig. 2b).

3.2. X-ray diffraction and Rietveld structure refinement

In order to assign the DSC exothermic events, the heating in DSC apparatus was stopped after each exothermic peak, the specimen was quenched and submitted to X-ray diffraction analysis. XRD patterns of quenched specimens for non-doped sample are shown in Fig. 3. The temperatures at which DSC runs were stopped and the samples subsequently quenched and performed to X-ray diffraction analysis are given in the picture. Broad Al–Si spinel lines are seen in the specimen quenched at 976 °C, whereas mullite lines occur in the pattern of specimen quenched from 1255 °C. At 1350 °C only mullite was observed.

XRD patterns of sample doped with 3 at.% Co^{2+} treated to different temperatures are given in Fig. 4. For the specimen quenched from 951 °C (after the first exothermic peak on DSC scan) only broadened lines of spinel are observed. As the spinel lines on XRD pattern were broadened, it is difficult to attribute them to any of the particular two spinel phases assumed on the basis of DSC data. Both phases: Al–Si spinel and $CoAl_2O_4$ have spinel structure, discerned only by a fact that Al–Si spinel has a defect spinel structure,[14] whereas $CoAl_2O_4$ has normal spinel

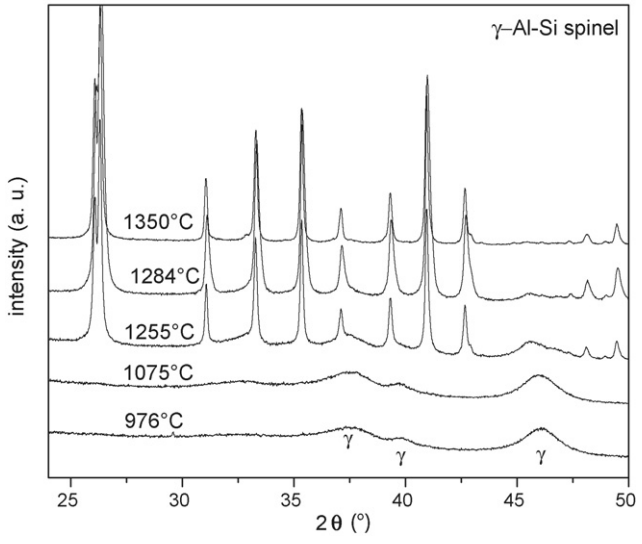

Fig. 3. X-ray diffraction patterns of non-doped calcined sample quenched in DSC at temperatures given in the picture. γ-Al–Si spinel. Mullite lines are not marked.

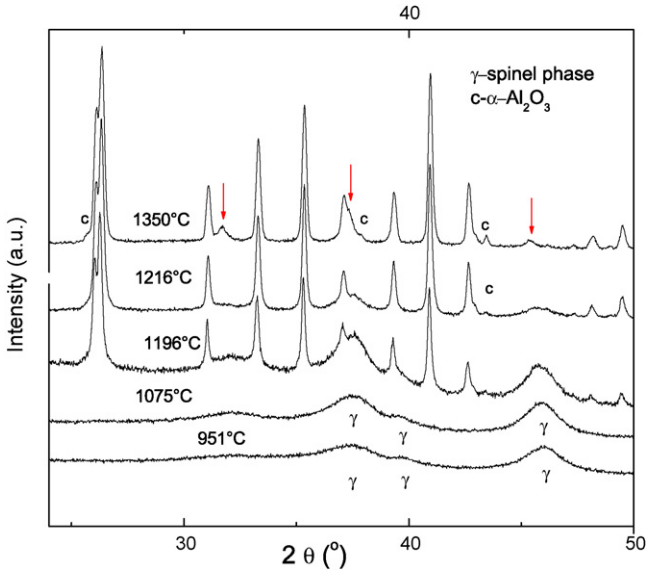

Fig. 4. X-ray diffraction patterns of Co3 (3 at.% Co^{2+}) sample quenched in DSC at temperatures given in the picture. Lines of $CoAl_2O_4$–Al_2O_3 solid solution are marked with arrows. c-α-Al_2O_3 (corundum).

structure and is characterized by well defined sharp lines. Even the prolonged heat treatment at 900 °C (not shown here) did not resolve the above problem. Only after the reaction of Al–Si spinel with amorphous silica and formation of mullite at about 1200 °C, solid solution of $CoAl_2O_4$–Al_2O_3 ($a = 8.032(5)$ nm) was determined with certainty. It is interesting to mention that at 1350 °C powder is partially sintered and SEM micrograph and EDX analysis (Fig. 5) show that in the grains separated from the matrix; cobalt, aluminum and oxygen dominated, whereas in the sintered matrix alumina and silica dominate.

Diffraction patterns between 10° and 100° 2θ of annealed samples with silicon as a standard were used for determination of mullite and $CoAl_2O_4$ unit cell parameters. Obtained values were than used as input data in Rietveld refinement. XRD patterns between 10–45° 2θ of annealed samples are shown in Fig. 6. Refined lattice parameters for mullite and $CoAl_2O_4$ are shown in Fig. 7. Rietveld output of X-ray powder pattern data for Co3 sample is given in Fig. 8, as an example. In the case of cobalt doped samples, refinement was started using mullite structure model,[11] in which 2a octaehedral sites were occupied by both atoms (aluminium an cobalt) under the constraints that full occupancy of the site is equal 1. Results of quantitative analyses and details of Rietveld refinement for Co0, Co1, Co2 and Co3 samples are summarized in Table 3. The effect of the cobalt to refinement was negligible; no smaller R_{wp} factors were obtained. Ratio between $CoAl_2O_4$ quantity found in annealed samples and Co^{2+} doping level in gels is shown in Fig. 9.

4. Discussion

4.1. DSC analysis and determination of activation energy for crystallization of spinels and mullite

As shown in Fig. 1 dried gels exhibited two exothermic events in the temperature range of spinel crystallization; the

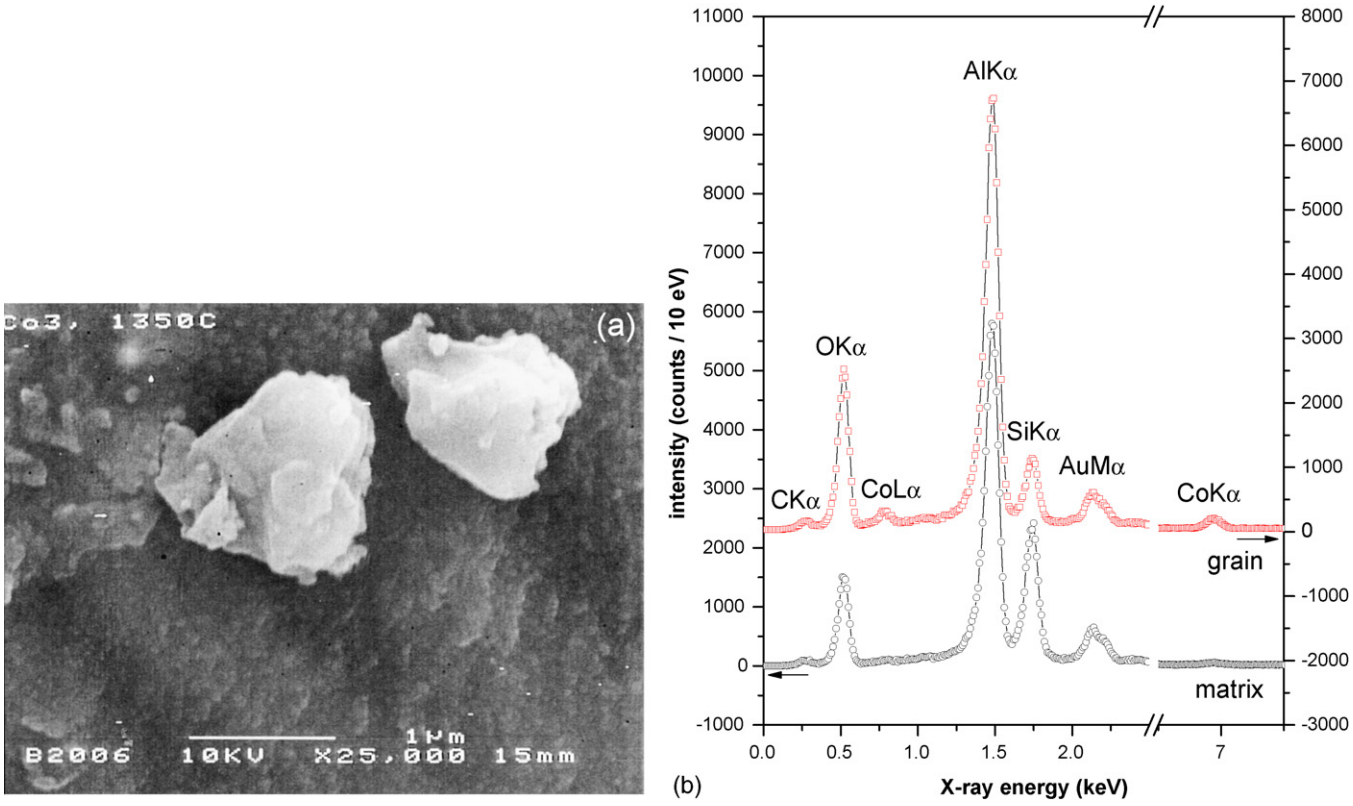

Fig. 5. SEM micrograph (a) and EDX analysis (b) of sample partially sintered and 1350 °C.

first peak is increased with the increase of cobalt content in the gels. It was reported[7] that solid solutions of γ-Al_2O_3 and $CoAl_2O_4$ can be prepared by sol–gel technique, and some initial crystallinity of spinel-type structure can appear from 250 °C upward. Therefore, it can be supposed that during the DSC run of dried gels, and after the nitrate decomposition, γ-Al_2O_3 with some cobalt incorporated in the structure crystallizes first, followed by Al–Si spinel. The two different exothermic events observed are most likely the result of phase separation, which is enlarged in comparison with non-doped samples due to cobalt incorporation in the system. Studying the spinel crystallization in Ni-doped diphasic gels with mullite composition[15] we also found two individual spinel peaks and lower activation energy of crystallization for the first spinel phase (E_{a1}) than for the second spinel (E_{a2}). The E_{a1} and E_{a2} in Cod3 diphasic pre-mullite gel were found to be 822 ± 64 and 1173 ± 15 kJ mol^{-1}, respectively (Table 2). To the best of our knowledge we could

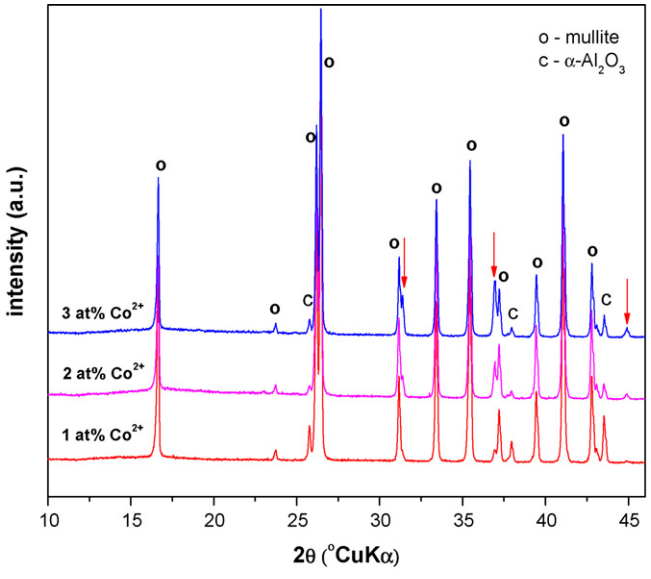

Fig. 6. XRD patterns of Co1, Co2 and Co3 samples annealed at 1600 °C for 2 h. 012, 110 and 113 lines of α-Al_2O_3 (corundum) are marked as c (other corundum lines in the range of 30–45° are overlapped with mullite lines or to small and are not marked). The 111, 220 and 400 lines of $CoAl_2O_4$ are marked with arrows.

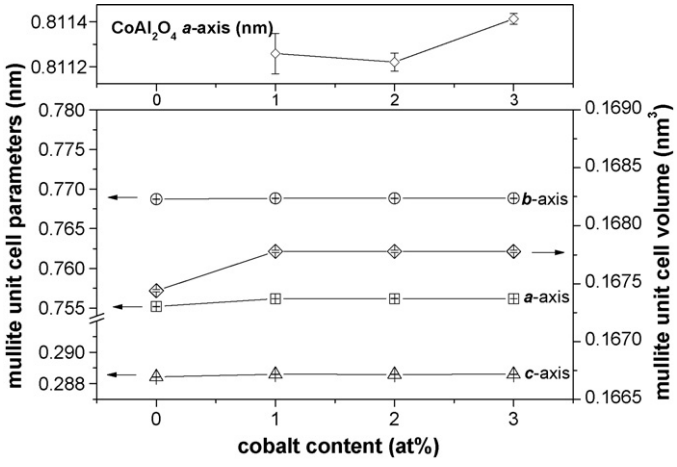

Fig. 7. Mullite and $CoAl_2O_4$ unit cell parameters vs. Co^{2+} content.

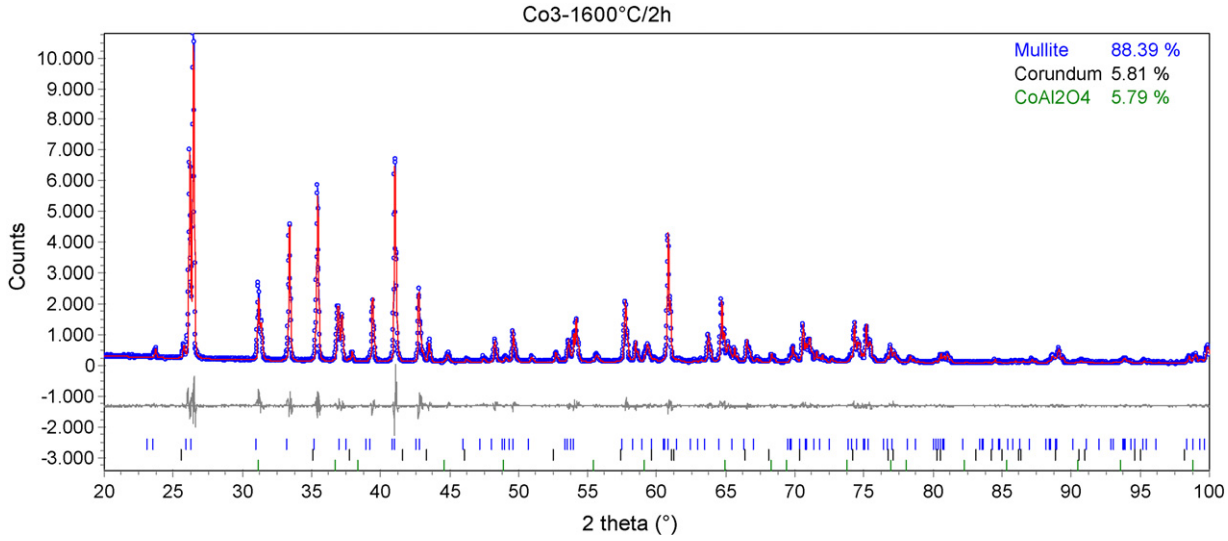

Fig. 8. Rietveld output of X-ray powder pattern of Co3 sample heat-treated at 1600 °C for 2 h. The solid line is the best-fit profile, and dots superimposed on it are the experimental data. The difference between experimental and fitted pattern is shown under the diffraction pattern. Line markers on the bottom of the figure indicate the position of Bragg reflections for mullite, $CoAl_2O_4$ and corundum.

not find data for the activation energy of crystallization for $CoAl_2O_4$ or solid solutions of $CoAl_2O_4$–Al_2O_3. On the other hand, the activation energy for Al–Si spinel crystallization (E_{a2}) is in accordance with that found for Al–Si spinel crystallization in non-doped diphasic gels.[16]

The overlapping of two spinel peaks occurs due to homogenization of the calcined gels, as seen in Fig. 1b. Two compositionally different phases have different kinetics of crystallization. Therefore, at different heating rates the degree of overlapping for corresponding exothermic peaks is different, causing irregular shift of apparent T_p with the heating rate. Consequently, the $\ln(\beta/T_p^2)$ value is also shifted non-linearly with the reciprocal temperature (as seen in Fig. 2c), which disables the application of Kissinger method to overlapped spinel scans of calcined samples. Studying the devitrification kinetics of quenched mullite beads, Johnson et al.[17] have observed two overlapping mullite exothermic events and the shift in dominance one of them dependent on the heating rate of DSC run. The same phenomenon could occur by spinel crystallization too. Activation energy for mullite crystallization was evaluated on calcined samples, since they contained smaller amount of volatiles (lower mass loss), and mullite peaks are more pronounced; consequently more precise T_p values can be determined.

4.2. X-ray analysis and Rietveld structure refinement

XRD patterns of non-doped and cobalt doped samples are alike up to ~1200 °C (Figs. 3 and 4). They exhibit broad peaks that can be attributed to slight crystalline spinel-type structure, but the incorporation of Co^{2+} in the first spinel phase cannot be confirmed by XRD. Recently, nanocrystaline $CoAl_2O_4$ at about 500 °C was obtained by sol–gel method[7] using $Co(NO_3)_2{\cdot}4H_2O$ and $Al(NO_3)_3{\cdot}9H_2O$ as precursors. The same authors proposed several steps of $CoAl_2O_4$ formation: transformation of precursors in amorphous phase with spinel composition, nucleation of crystalline cobalt aluminate in the amorphous matrix and grain growth of $CoAl_2O_4$ by solid-state reaction. We propose the similar mechanism for crystallization of cobalt aluminate in the Al_2O_3–SiO_2 system studied in this work, but with some modifications. The mullite formation mechanism in stoichiometric and undoped diphasic mullite gels (using TEOS and aluminum

Table 3
Results for quantitative analyses (wt.%) and details of Rietveld refinement for samples Co0, Co1, Co2 and Co3 heated at 1600 °C for 2 h

	Co0	Co1	Co2	Co3
Doping level (at.%)	0	1	2	3
Reliability factors (%)				
R_p	9.36	7.65 (7.55)	7.72 (7.73)	8.22 (8.21)
R_{wp}	12.31	10.37 (10.33)	10.45 (10.46)	11.04 (11.02)
R_{exp}	5.61	5.29 (5.26)	5.28 (5.28)	5.51 (5.51)
Mullite	94.2	88.5 (88.8)	93.3 (93.8)	88.4 (88.4)
Corundum (α-Al_2O_3)	5.8	10.3 (10.3)	3.8 (3.4)	5.8 (5.8)
$CoAl_2O_4$	–	0.8 (0.8)	2.9 (2.9)	5.8 (5.8)

Numbers in parentheses correspond to fitting data assuming no cobalt incorporation in mullite structure.

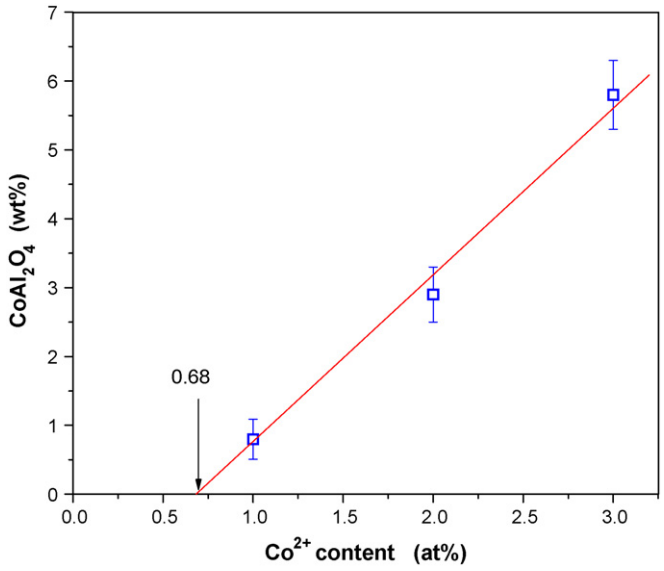

Fig. 9. The amount of $CoAl_2O_4$ in annealed samples vs. Co^{2+} content in gels.

nitrate) has been already proposed.[18] Al–Si spinel (solid solution of γ-Al_2O_3 and silica) is the first crystalline phase in diphasic non-doped gels with mullite composition. It is a metastable phase and reacts with SiO_2-rich amorphous phase to form mullite above 1200 °C (Fig. 3). In the doped samples, however, the first faint crystalline phase is γ-Al_2O_3 with cobalt incorporation. Its formation shifts the Al–Si spinel crystallization to lower temperatures. Consequently, the reaction of Al–Si spinel with silica-rich amorphous phase producing mullite occurs below 1200 °C (Fig. 4). Cobalt-containing γ-Al_2O_3 transforms progressively (forming $CoAl_2O_4$-solid solution with different unit cell parameters) in $CoAl_2O_4$ at 1600 °C.

Described path leads to morphology showed in SEM micrograph (Fig. 5a). According to EDX analysis (Fig. 5b) coarse grains separated from the matrix are rich in cobalt while the sintered matrix has mullite composition.

The refined mullite lattice parameters obtained (Fig. 7) are similar for all doped mullite samples regardless of Co^{2+} quantity. However, *a*-axis of mullite in cobalt doped samples is significantly greater than *a*-axis of mullite in undoped sample According to literature data[19] it could be expected that Co^{2+} (ionic radius of 0.75 Å) substituted for Al^{3+}(ionic radius of 0.53 Å) in the AlO_6 octahedra of the mullite structure would increase the mullite *c*-axis. However, that is not the case. Mullite in doped samples is characterized with larger *a*-axis than that in undoped sample. It also has to be noticed that the reliability factor R_{wp} is constant regardless whether in the mullite structure model Co^{2+} was located in M1 position of AlO_6 octahedra or not (Table 3). From the relation between quantities of $CoAl_2O_4$ found by Rietveld refinement in annealed samples and content of cobalt in the gels (Fig. 9) it can be estimated that about 0.6 at.% Co^{2+} does not crystallize as spinel. The question is whether it is incorporated in mullite or in the glassy phase, which always exists in small quantities in the system. If cobalt is incorporated in mullite structure it is beyond the resolution of Rietveld refinement method.

5. Conclusion

DSC analyses and the activation energy determinations for spinel crystallization have shown that in Co-doped diphasic gels the phase separation is intensified in comparison to non-doped amorphous precursors with mullite composition. Two defect spinel phases crystallize, having different composition and activation energies. The former phase, with smaller activation energy is attributed to defect spinel structure with cobalt incorporation and the latter to Al–Si spinel.

Mullite lattice parameters and Rietveld structure refinements of powder XRD data suggest that Co^{2+} could be incorporated in mullite structure but in very small amounts affecting no change of any of reliability factors which characterize a quality of fitting results.

The ratio of $CoAl_2O_4$ quantities in annealed mullite samples (at 1600 °C for 2 h) and total Co^{2+} content in gels points out that the majority of cobalt crystallizes as $CoAl_2O_4$ and only about 0.6 at.% remains in the system, entering mullite structure or the glassy phase, or both.

References

1. Aksay, I. A., Dabbs, D. M. and Sarykaya, M., Mullite for structural, electronic, and optical applications. *J. Am. Ceram. Soc.*, 1991, **74**, 2343–2358.
2. Schneider, H., Okada, K. and Pask, J., *Mullite and Mullite Ceramics*. John Wiley & Sons, Chichester, 1994, pp. 38–63.
3. Sales, M., Valentin, C. and Alarcón, J., Spinel–mullite composites with optical properties. *J. Sol–Gel Sci. Technol.*, 1997, **8**, 871–875.
4. Sales, M., Valentin, K. and Alarcón, J., Cobalt aluminate spinel–mullite composites synthesized by sol–gel method. *J. Eur. Ceram. Soc.*, 1997, **17**, 41–47.
5. Mazza, D., Delmastro, A., Ronchetti, S. and Co, Ni, Cu aluminates supported on mullite precursors via a solid state reaction. *J. Eur. Ceram. Soc.*, 2000, **20**, 699–706.
6. Cho, W.-S. and Kakihana, M., Crystallization of ceramic pigment $CoAl_2O_4$ nanocrystals from Co–Al metal organic precursor. *J. Alloys Compd.*, 1999, **287**, 87–90.
7. Arean, C. O., Mentruit, M. P., Platero, E. E., Xamena, F. X. L. and Parra, J. B., Sol–gel method for preparing high surface area $CoAl_2O_4$ and Al_2O_3–$CoAl_2O_4$ spinels. *Mater. Lett.*, 1999, **39**, 22–27.
8. Kissinger, H. E., Variation of peak temperature with heating rate in differential thermal analysis. *J. Res. Natl. Bur. Stand. (US)*, 1956, **57**(4), 217–221.
9. Young, R. A., The Rietveld method, international union of crystallography. *Monographs on Crystallography*, *5*. Oxford Press, Oxford, 1993.
10. Bruker, *Advanced X-ray Solutions, TOPAS 2.1*, 2003.
11. Ban, T. and Okada, K., Structure refinement of mullite by Rietveld method and a new method for estimation of chemical composition. *J. Am. Ceram. Soc.*, 1992, **75**, 227–230.
12. O'Neil, H. S. C., Temperature dependence of the cation distribution in $CoAl_2O_4$ spinel. *Eur. J. Miner.*, 1994, **6**, 603–609.
13. Ballirano, P. and Caminiti, R., Rietveld refinement on laboratory energy dispersive X-ray diffraction data (EDXD). *J. Appl. Crystallogr.*, 2001, **34**, 757–762.
14. Gerardin, C., Sundaresan, S., Banzinger, J. and Navrotsky, A., Structural investigation and energetics of mullite formation from sol–gel precursors. *Chem. Mater.*, 1994, **6**, 160–170.
15. Kurajica, S. and Tkalcec, E., $NiAl_2O_4$–mullite composites prepared by sol–gel processes. In *Proceedings of the Forth International Conference on Inorganic Materials*, 2004, p. 154 [Abstract book].

16. Tkalcec, E., Kurajica, S. and Ivankovic, H., Diphasic aluminosilicate gels with two stage mullitization in temperature range of 1200–1300 °C. *J. Eur. Ceram. Soc.*, 2005, **25**, 613–625.
17. Johnson, B. R., Kriven, W. M. and Schneider, J., Crystal structure development during devitrification of quenched mullite. *J. Eur. Ceram. Soc.*, 2001, **21**, 2541–2562.
18. Schneider, H., Voll, D., Saruhan, B., Sanz, J., Schraeder, G., Ruescher, C. and Mosset, A., Synthesis and structural characterization of non-crystalline mullite precursors. *J. Non-Cryst. Solids*, 1994, **78**, 262–271.
19. Schneider, H., Transition metal distribution in mullite. In *Ceramics Transactions, Mullite and Mullite Matrix Composites*, *6*, ed. S. Somiya, R. F. Davis and J. A. Pask. American Ceramic Society, Westerville, OH, 1990, pp. 135–157.